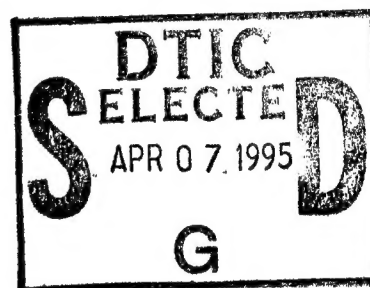


NAVAL POSTGRADUATE SCHOOL MONTEREY, CALIFORNIA



THESIS



THERMAL ANALYSIS OF THE ADVANCED
LIGHTWEIGHT INFLUENCE SWEEP SYSTEM
(ALISS) SUPERCONDUCTING MAGNET

by

Phillip K. Pall

December, 1994

Thesis Advisor:

M. D. Kelleher

Approved for public release; distribution is unlimited.

19950406 059

DTIC QUALITY INSPECTED 5

REPORT DOCUMENTATION PAGE			Form Approved OMB No. 0704-0188	
Public reporting burden for this collection of information is estimated to average 1 hour per response, including the time for reviewing instruction, searching existing data sources, gathering and maintaining the data needed, and completing and reviewing the collection of information. Send comments regarding this burden estimate or any other aspect of this collection of information, including suggestions for reducing this burden, to Washington Headquarters Services, Directorate for Information Operations and Reports, 1215 Jefferson Davis Highway, Suite 1204, Arlington, VA 22202-4302, and to the Office of Management and Budget, Paperwork Reduction Project (0704-0188) Washington DC 20503.				
1. AGENCY USE ONLY (Leave blank)	2. REPORT DATE December 1994.	3. REPORT TYPE AND DATES COVERED Master's Thesis		
4. TITLE AND SUBTITLE : THERMAL ANALYSIS OF THE ADVANCED LIGHTWEIGHT INFLUENCE SWEEP SYSTEM (ALISS) SUPERCONDUCTING MAGNET		5. FUNDING NUMBERS		
6. AUTHOR PHILLIP K. PALL				
7. PERFORMING ORGANIZATION NAME(S) AND ADDRESS(ES) Naval Postgraduate School Monterey CA 93943-5000		8. PERFORMING ORGANIZATION REPORT NUMBER		
9. SPONSORING/MONITORING AGENCY NAME(S) AND ADDRESS(ES)		10. SPONSORING/MONITORING AGENCY REPORT NUMBER		
11. SUPPLEMENTARY NOTES The views expressed in this thesis are those of the author and do not reflect the official policy or position of the Department of Defense or the U.S. Government.				
12a. DISTRIBUTION/AVAILABILITY STATEMENT Approved for public release; distribution is unlimited.		12b. DISTRIBUTION CODE		
13. ABSTRACT (maximum 200 words) A steady state thermal analysis of the superconducting magnet (SCM) in the Advanced Lightweight Influence Sweep System (ALISS) was performed using commercial Finite Element Modeling (FEM) software. Cryocooler interface temperature from a no-load performance curve and uniform heat flux due to radiation, conduction and instrumentation heat leaks were input as the boundary conditions. Two major cases were examined: one with instrumentation heat flux dispersed around the SCM and one with instrumentation heat flux concentrated. Both resulted in the SCM staying within temperature specifications. A separate group of exploratory cases determined the heat flux values that "quenched" the SCM, causing cessation of superconductivity.				
14. SUBJECT TERMS: Superconductivity, Superconducting Magnets, ALISS			15. NUMBER OF PAGES 50	
			16. PRICE CODE	
17. SECURITY CLASSIFICATION OF REPORT Unclassified	18. SECURITY CLASSIFICATION OF THIS PAGE Unclassified	19. SECURITY CLASSIFICATION OF ABSTRACT Unclassified	20. LIMITATION OF ABSTRACT UL	

NSN 7540-01-280-5500

Standard Form 298 (Rev. 2-89)

Prescribed by ANSI Std. Z39-18 298-102

Approved for public release; distribution is unlimited.

**THERMAL ANALYSIS OF THE ADVANCED LIGHTWEIGHT
INFLUENCE SWEEP SYSTEM (ALISS) SUPERCONDUCTING MAGNET**

by

Phillip K. Pall
Lieutenant, United States Navy
B.S., United States Naval Academy, May 1986

Submitted in partial fulfillment
of the requirements for the degree of

MASTER OF SCIENCE IN MECHANICAL ENGINEERING

from the

NAVAL POSTGRADUATE SCHOOL
December 1994

Author:

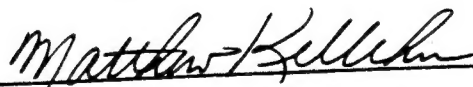


Phillip K. Pall

Approved by:



M. D. Kelleher, Thesis Advisor



M. D. Kelleher, Chairman
Department of Mechanical Engineering

ABSTRACT

A steady state thermal analysis of the superconducting magnet (SCM) in the Advanced Lightweight Influence Sweep System (ALISS) was performed using commercial Finite Element Modeling (FEM) software. Cryocooler interface temperature from a no-load performance curve and uniform heat flux due to radiation, conduction and instrumentation heat leaks were input as the boundary conditions. Two major cases were examined: one with instrumentation heat flux dispersed around the SCM and one with instrumentation heat flux concentrated. Both resulted in the SCM staying within temperature specifications. A separate group of exploratory cases determined the heat flux values that "quenched" the SCM, causing cessation of superconductivity.

Accession For	
NTIS	CRA&I <input checked="checked" type="checkbox"/>
DTIC	TAB <input type="checkbox"/>
Unannounced <input type="checkbox"/>	
Justification _____	
By _____	
Distribution /	
Availability Codes	
Dist	Avail and/or Special
A-1	

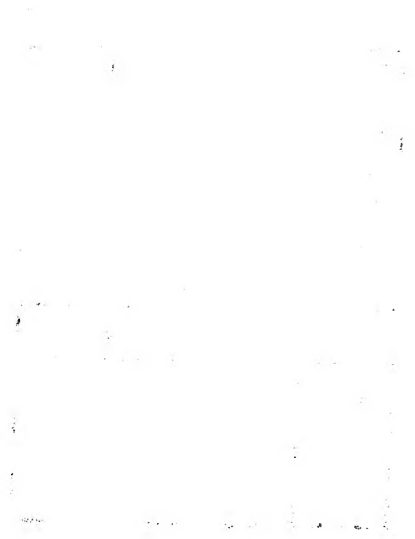


TABLE OF CONTENTS

I.	INTRODUCTION	1
	A. U. S. NAVY MINE COUNTERMEASURES	1
	B. SUPERCONDUCTIVITY	2
	C. ALISS SUPERCONDUCTING MAGNET	4
	D. OBJECTIVE	8
II.	FINITE ELEMENT MODEL	9
	A. GENERAL	9
	B. GEOMETRIC MODEL	10
	C. BOUNDARY CONDITIONS	15
III.	RESULTS	21
	A. GENERAL	21
	B. DISPERSED INSTRUMENTATION HEAT FLUX CASE . . .	21
	C. CONCENTRATED INSTRUMENTATION HEAT FLUX CASE .	25
	D. EXPLORATORY QUENCH CASES	29
IV.	DISCUSSION	31
	A. CONCLUSIONS	31
	B. RECOMMENDATIONS	31
	LIST OF REFERENCES	33
	INITIAL DISTRIBUTION LIST	35

LIST OF TABLES

Table 1:	SCM Component Physical Dimensions	8
Table 2:	Thermal Conductivity Functions for SCM Components .	14
Table 3:	Dispersed Instrumentation Heat Flux Case Boundary Conditions	20
Table 4:	Concentrated Instrumentation Heat Flux Case Boundary Conditions	20
Table 5:	Exploratory Case Results	29

LIST OF FIGURES

Figure 1a:	Diagram of SCM (Top View)	6
Figure 1b:	Diagram of SCM (Side View)	7
Figure 2:	Wire Diagram of View 1 of Bisected SCM	11
Figure 3:	Wire Diagram of View 2 of Bisected SCM	12
Figure 4:	Wire Diagram of View 3 of Bisected SCM	13
Figure 5:	Arrangement of Elements and Nodes in Bisected SCM	17
Figure 6:	Cryocooler No-load Performance Curve	18
Figure 7:	Dispersed Instrumentation Heat Flux Case Temperature Profile (View 1)	22
Figure 8:	Dispersed Instrumentation Heat Flux Case Temperature Profile (View 2)	23
Figure 9:	Dispersed Instrumentation Heat Flux Case Temperature Profile (View 3)	24
Figure 10:	Concentrated Instrumentation Heat Flux Case Temperature Profile (View 1)	26
Figure 11:	Concentrated Instrumentation Heat Flux case Temperature Profile (View 2)	27
Figure 12:	Concentrated Instrumentation Heat Flux Case Temperature Profile (View 3)	28

ACKNOWLEDGMENT

The author would like to express his sincere gratitude to the following people who helped make this thesis possible:

- Professor Kelleher, the thesis advisor, who patiently provided guidance and direction.

- Annapolis Detachment (Carderock Division, Naval Surface Warfare Center), for financial support.

- Dr. Joe Walters, of the Annapolis Detachment, for his invaluable help and advice.

- Mary Pall, the author's wife, for her encouragement and support.

I. INTRODUCTION

A. U. S. NAVY MINE COUNTERMEASURES

Historically, the United States Navy has had a great deal of difficulty in maintaining its capabilities in mine countermeasures (MCM). For example, nearly thirty years passed before the USS AVENGER (MCM-1) class began to replace the Korean War MSOs (Ocean-going Minesweepers) [Ref. 1]. Though the U. S. Navy has always advocated a balanced fleet, the composition of that balance depends on the perceived threat. During the Cold War, when MCM competed for scarce resources against higher priority programs, it typically came out the loser [Ref. 2]. However, since the collapse of the Soviet threat, and with unpleasant memories of several Persian Gulf mine incidents, the U. S. Navy is placing MCM among its highest priorities.

Ranging from the acquisition of new ships and aircraft to revision in doctrine, training and organization, the Navy is moving to create a more capable and responsive MCM force. The MCM force required by today's focus on the littoral environment that encompasses the coastlines of some 122 nations [Ref. 3]. Despite the end of the Cold War, the possibility of U.S. military intervention in response to regional crises has far from diminished. Amphibious assault and its supporting strategic sealift are considered more important than ever [Ref. 4]. Unfortunately, the threat from sea mines has become more lethal. Sea mines pose a grave and proven danger to surface vessels, especially during littoral warfare operations. The breakup of the Soviet Union promises to accelerate the transfer of mines to Third World countries, some of which have long threatened western naval forces [Ref. 5]. All contact and many influence type mines are readily available for sale from a number of sources to nearly any country that wishes to use them. Influence mine casings can

be manufactured out of practically any material and are easily disguised as rocks or bottom debris. Quite sophisticated devices can be produced in simple workshops by a nation having relatively limited technological and financial capability [Ref. 6]. Though the improvement and refinement of existing MCM equipment continue, a revolutionary rather than evolutionary move must be made. Current magnetic influence mine countermeasures systems suffer from serious limitations and disadvantages given the expanding threat [Ref. 7]. To keep ahead of this threat, the Navy is applying new technology in the development of MCM. One such program is the Advanced Lightweight Influence Sweep System (ALISS). It uses superconducting magnets to sweep magnetic influence mines.

B. SUPERCONDUCTIVITY

Superconductivity is a phenomenon in which a material conducts electricity without resistance. This was first observed in 1911 by Professor Heike Kamerlingh Onnes of the University of Leiden in Holland. In working with frozen mercury, he had originally thought that electrical resistance would decrease continuously with falling temperature and then vanish at zero degrees Kelvin. Instead, he found mercury's electrical resistance disappeared sharply at 4.15 degrees Kelvin. The existence of a new state of mercury, characterized by the absence of electrical resistivity, was recognized by the scientific community and termed the superconducting state. In 1913, Professor Onnes was honored with the Nobel Prize in Physics for his discovery. Unfortunately, progress in the comprehension and application of superconductivity soon fell to a slow but steady crawl. The modern theory of superconductivity was developed in the 1950s by three American physicists: John Bardeen, Leon N. Cooper and John Robert Schrieffer. The B-C-S theory explains that a superconductor has no electrical resistance because of

an attractive interaction between its electrons that results in the formation of pairs of electrons. These "Cooper pairs" are bound to one another and flow without resistance around impurities and other imperfections. In an ordinary conductor, resistance occurs because its unbound electrons collide with imperfections and then scatter. In 1972, all three physicists received the Nobel Prize in Physics for their work. [Ref. 8]

Over a thousand metals and compounds are known to exhibit superconductivity. Each material has a three-parameter envelope defined by critical values of temperature, electrical current density and magnetic field intensity within which superconductivity occurs. Changes in one parameter affect the other parameters and the total result can be the cessation of superconductivity. Depending on the application, the cessation of superconductivity can be disastrous. In a charged superconducting magnet, any local rise in temperature above the critical temperature can soon create a runaway process in which the magnet will "quench." Any region of the SCM above the critical temperature will transform back to its normal resistive state. Joulean heating occurs due to the current flowing through the resistive region which spreads through the SCM causing a propagative increase of resistance and more subsequent Joulean heating. If the current supply is not immediately switched off, portions of the magnet can melt and cause catastrophic damage. [Ref. 9]

The critical currents and critical fields for the metals Onnes and his contemporaries were using were very low and prevented any useful application of superconductivity. The interest in superconductivity intensified in the early 1960s with the discovery of "high-field" superconductors. These were capable of keeping their zero electrical resistance in large magnetic fields well above 100 kiloGauss while simultaneously transmitting usefully large currents. [Ref. 10]

Work toward overcoming the heat transfer and material science obstacles involved in expanding superconductivity to a wider range of applications is well underway. Cryocoolers, super insulation and other heat transfer related components have significantly decreased the temperature at which we can maintain the superconducting state. Similarly, metallurgists are studying ways to improve the mechanical strength of the new breeds of high critical temperature superconducting materials [Ref. 11]. Advances in superconducting technology over the last twenty years have made it feasible to build a superconducting mine countermeasures (SCMCM) system.

C. ALISS SUPERCONDUCTING MAGNET

The U. S. Navy discussed using superconductivity in mine countermeasures as early as 1970 [Ref. 12]. ALISS now represents the premier research and development effort toward deploying an SCMCM system to the fleet. ALISS provides the dual capability to sweep both acoustic and magnetic influence mines. An acoustic subsystem contains the equipment necessary to transmit acoustic signals into the water to detonate acoustic influence mines. The magnetic subsystem will contain the part of ALISS that defeats magnetic influence mines. The magnetic subsystem's basic components are the refrigerator unit, electrical current unit and the cryostat.

Though many earlier superconducting magnets were kept cold by immersion in liquid helium, ALISS uses direct thermo-mechanical connection via a cryocooler interface between the SCM and an external refrigerator. Thus, the ALISS superconducting magnet is cooled solely by conduction. This change solves the logistical burden of supplying liquid helium to the deployed unit. There are two cryocoolers used in the refrigeration unit. Each is a closed-cycle two stage device, with the first stage being at the higher temperature. Cryocooler number one cools the SCM. Cryocooler number two is

dedicated solely for intercepting any conductive heat leak coming through the electrical current cables. This has been made possible by the recent development of refrigerators with the demanding low temperature performance required by ALISS.

The cryostat maintains the necessary environmental conditions to achieve superconductivity. The cryostat is a cylindrically shaped assembly containing the actual SCM structurally mounted to resist shock and vibration in an insulated vacuum chamber. It is composed of an aluminum outer shroud, radiation shields and layers of super insulation.

The SCM, as seen in Figures 1a and 1b, can be thought of as two concentric circular cylinders. Its dimensions are listed in Table 1. The inner circular cylinder is the aluminum inner bobbin. This is what the outer circular cylinder, the magnet, is wrapped around. The magnet is composed of a continuous strand of copper clad niobium-titanium (Nb-Ti) wire in an epoxy and fiberglass matrix. The copper cladding serves as a thermal and structural stabilizer. Nb-Ti is the most common and well-understood material for superconducting magnets. Nb-Ti offers a compromise between mechanical properties and superconductive properties. It is more ductile than other SCM materials, such as niobium-zirconium and niobium-tin. Therefore, it is easier to manufacture and fabricate into magnets but still has a satisfactory critical temperature of 10.5 K. [Ref. 13]

The cryocooler interface is connected to the aluminum inner bobbin along a 20 degree arc length of its outer edge as shown in Figure 1a. Another small arc length of this edge is where detachable electrical current leads are connected during minesweeping operations. The opposite outer edge of the aluminum inner bobbin is a structural support interface with the cryostat.

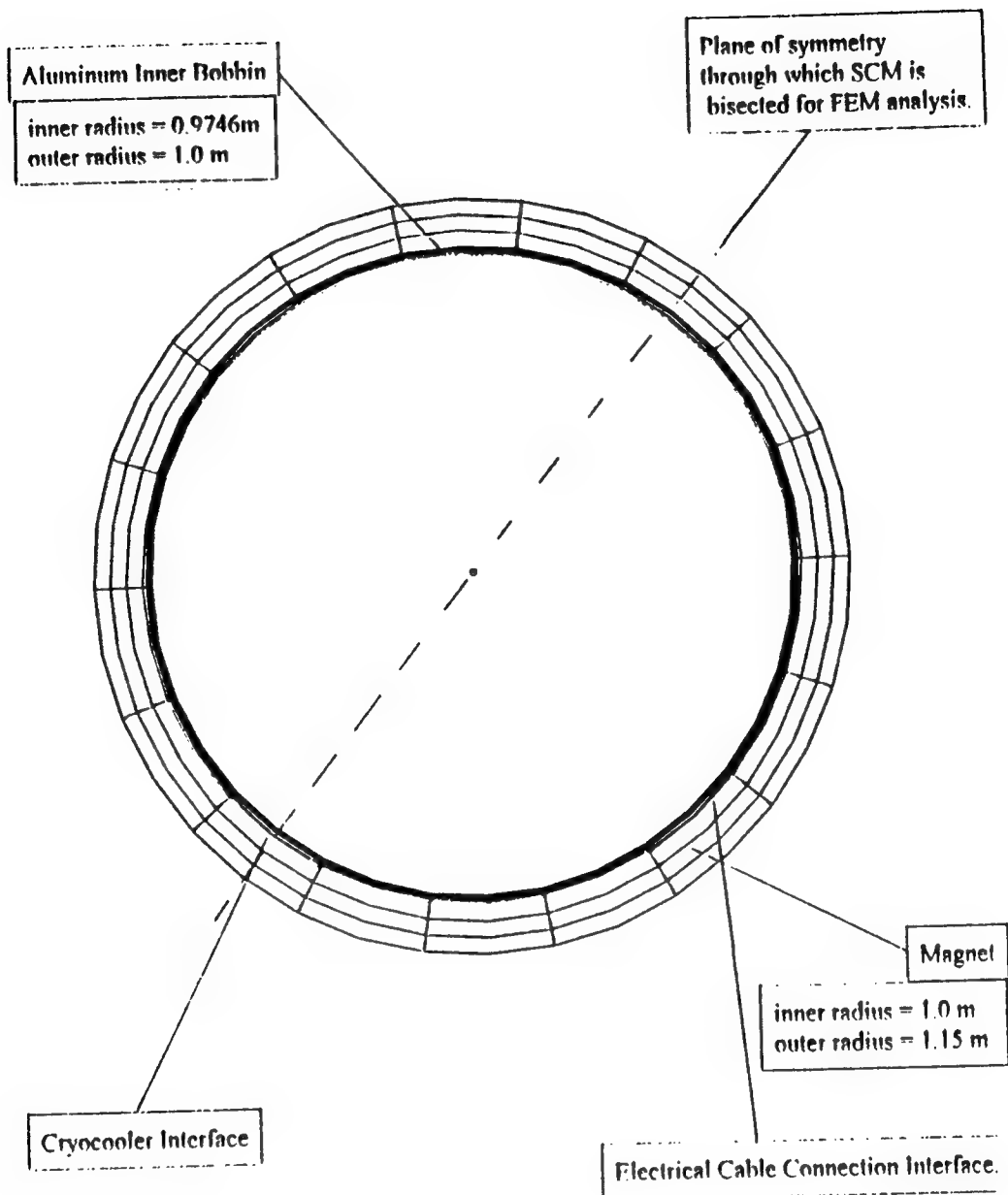


Figure 1a: Diagram of SCM (Top View)

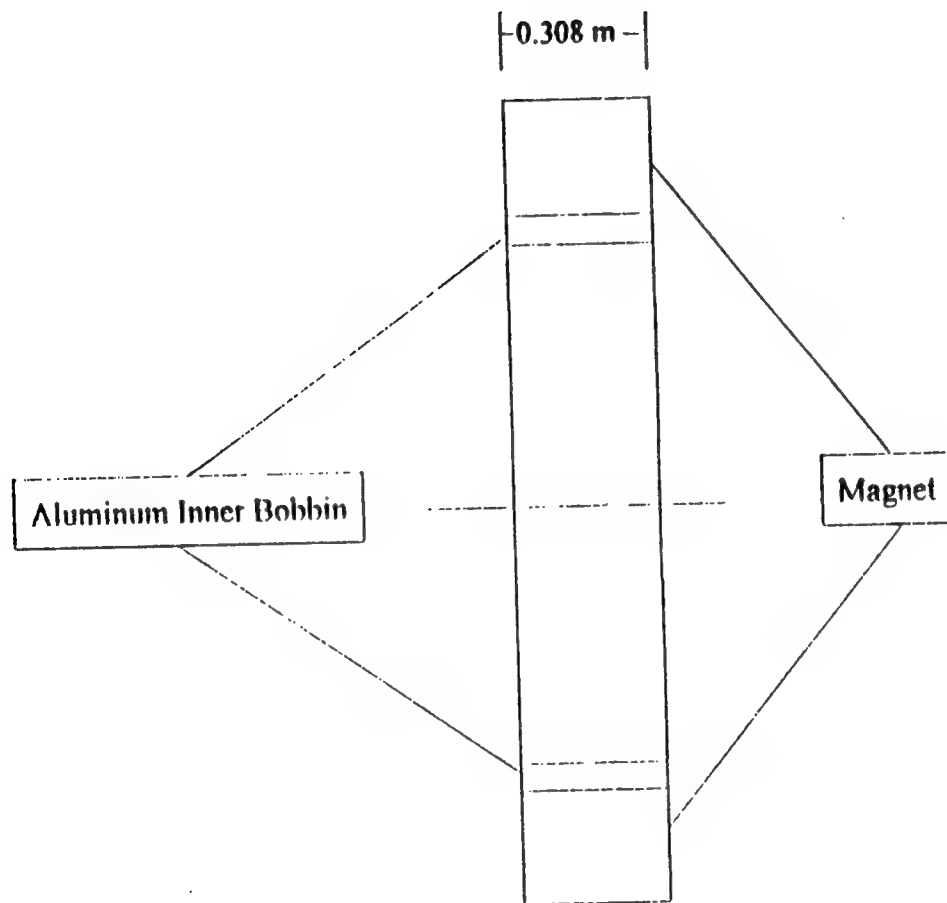


Figure 1b: Diagram of SCM (Side View)

Component	Inner Radius	Outer Radius	Thickness	Height
Al inner bobbin	0.9746 m	1.0 m	0.0254 m	0.308 m
magnet	1.0 m	1.15 m	0.15 m	0.308 m

Table 1: SCM Component Physical Dimensions

Heat leak by conduction occurs through this interface. The majority of the exposed outer surface of the SCM experiences a radiant heat flux. Instrumentation used in the monitoring of SCM parameters serves as a final heat leak path. The locations for this heat flux in the ALISS design have not been specified. Consideration of this fact leads to the analysis of two general cases for the location of the instrumentation heat flux. The dispersed case applies the instrumentation heat leak over a large number of elemental faces in the magnet's outer circumference. The concentrated case applies the heat leak on two adjacent elemental faces in the outer circumference of the magnet.

D. OBJECTIVE

The objective of this thesis was the thermal analysis of the superconducting magnet (SCM) designed for the U. S. Navy Advanced Lightweight Influence Sweep System (ALISS). ALISS is a research and development project to build a mine countermeasures system deployable onboard LCACs (Landing Craft, Air Cushion). It will sweep both magnetic and acoustic influence mines. The thermal analysis was conducted using the NISA family of commercial finite element (FEM) software provided by the thesis sponsor, Annapolis Detachment, Carderock Division Naval Surface Warfare Center (CDNSWC).

II. FINITE ELEMENT MODEL

A. GENERAL

All of the geometric and finite element modeling was conducted using NISA (Numerically Integrated elements for Systems Analysis) software. NISA is a family of commercially available programs using standard numerical methods to solve both structural and heat transfer problems [Ref. 14]. Thermal conductivities can only be entered in NISA for functions in a cartesian coordinate system. However, the magnet material in the SCM is an anisotropic material. It is orthotropic with three different thermal conductivity functions in a cylindrical coordinate system. NISA's inability to handle orthotropic thermal conductivities in a cylindrical coordinate system created a ceiling on the maximum number of nodes that could be implemented in the model.

The local coordinate axes for each node in the model had to be individually rotated a particular angle about the global cartesian coordinate z-axis. The rotation angle was that angle required for the node's local cartesian coordinate x-axis and y-axis to coincide with its local cylindrical coordinate azimuthal axis and radial axis respectively. Each node's local cartesian z-axis was already equivalent to its local cylindrical coordinate z-axis (axial direction) due to the chosen orientation of the model. In other words, the local cartesian x-y plane and the local cylindrical r- θ plane were always coplanar. Rotating each node's local cartesian coordinate axes was the only way to correctly model the thermal conductivities in NISA. Unfortunately, NISA could only manage approximately 4100 nodal axes rotations. This restricted the thermal analysis to a coarser mesh than would have otherwise been utilized. Additionally, the nodal rotation angles had to be manually typed into the NISA input file since DISPLAY III did not support the axes rotation

command entry. This hampered the ability to experiment with a large number of different mesh arrangements.

B. GEOMETRIC MODEL

This steady state thermal analysis will focus solely on the situation where current is not flowing in the electrical cables. Therefore, symmetry about the cryocooler interface allows the bisection of the SCM into two semicircular cylinders. This greatly simplified the geometric and finite element modeling. Figures 2 through 4 reiterate the locations of all of the SCM's main features on the semicircular cylinder used in the FEM analysis. The perspective of these figures are the same ones that will be used for the color temperature profiles. The items modeled in the semicircular control volume were the magnet, the aluminum inner bobbin, the cryocooler interface and the instrumentation interfaces on the outer circumference of the magnet. The magnet was modeled as an orthotropic material in a cylindrical coordinate system, with three different temperature dependent thermal conductivities in the axial, radial and azimuthal directions. The aluminum inner bobbin was modeled as an isotropic material in a cylindrical coordinate system with a single temperature dependent thermal conductivity. The functions for the magnet's axial and radial thermal conductivity and the aluminum inner bobbin's isotropic thermal conductivity functions were all provided by NSWC, Annapolis [Ref. 15]. As recommended by NSWC, the function for the magnet's azimuthal thermal conductivity was formulated using the low temperature thermal conductivity data of series-1100 aluminum [Refs. 16 and 17]. This was based on their experimental results being very similar to the aluminum data [Refs. 18 and 19]. Table 2 lists these temperature dependent functions. The functions are valid over a temperature range from 4 to 30 Kelvin.

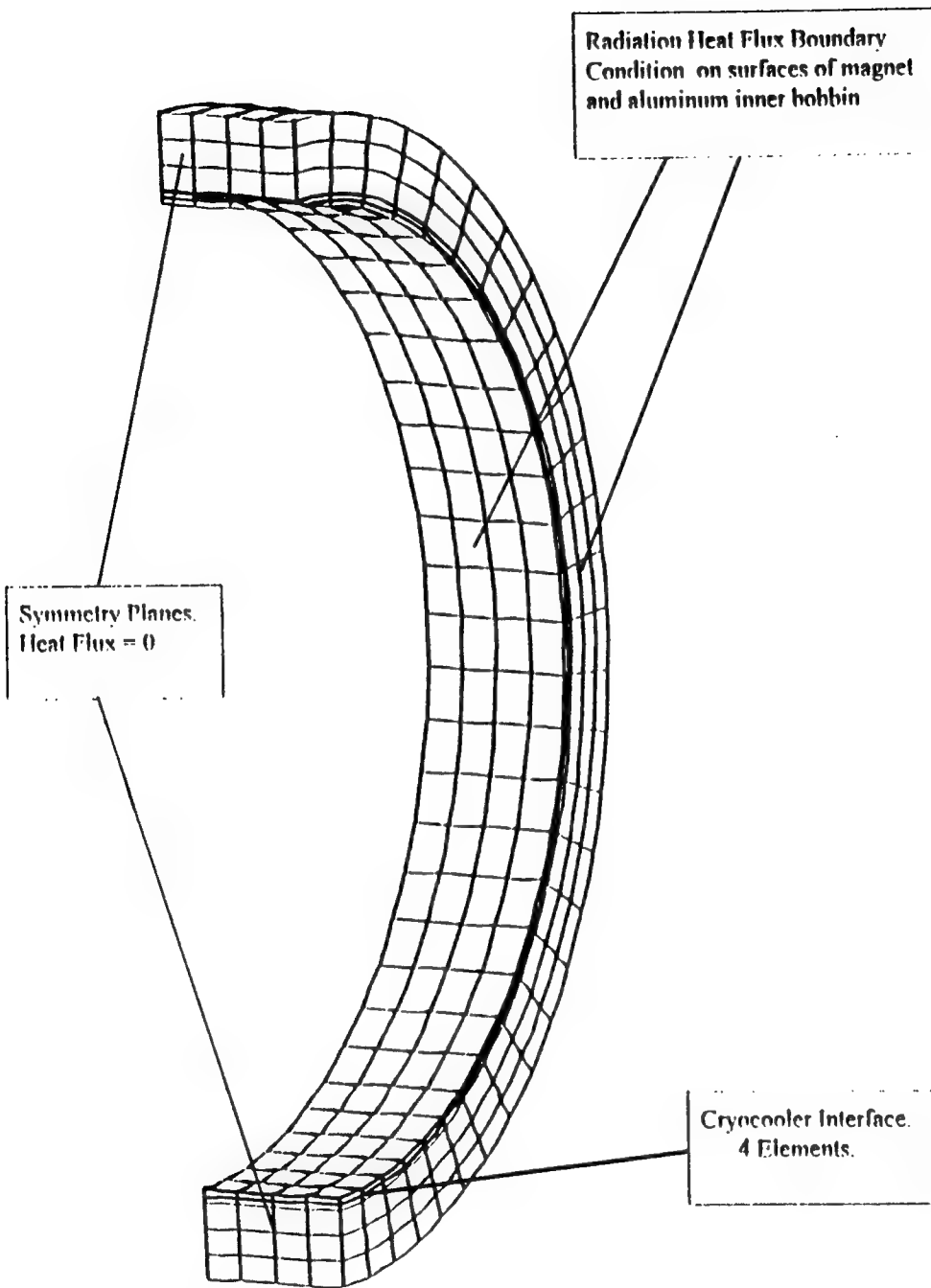


Figure 2: Wire Diagram of View 1 of Bisected SCM

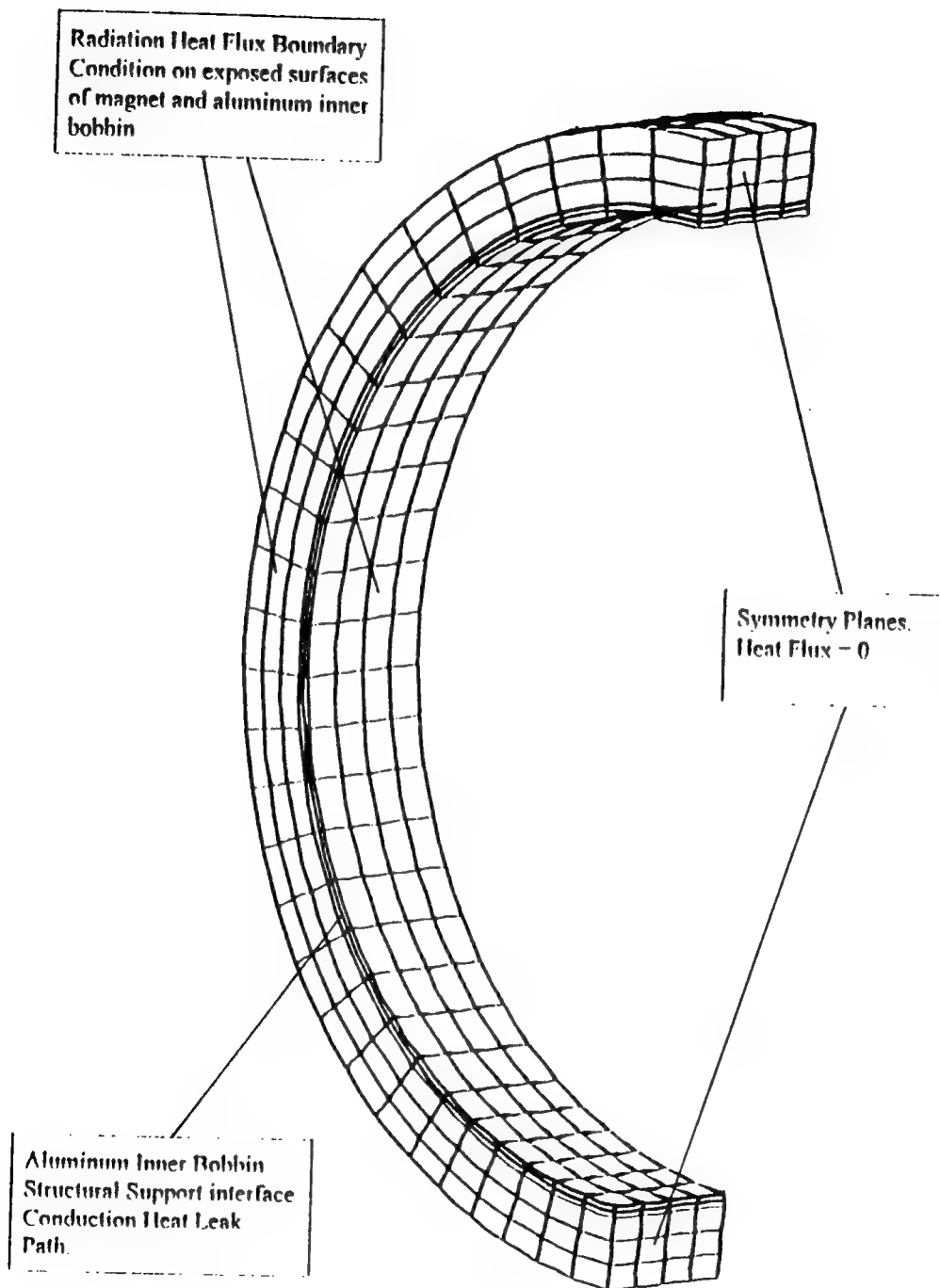


Figure 3: Wire Diagram of View 2 of Bisected SCM

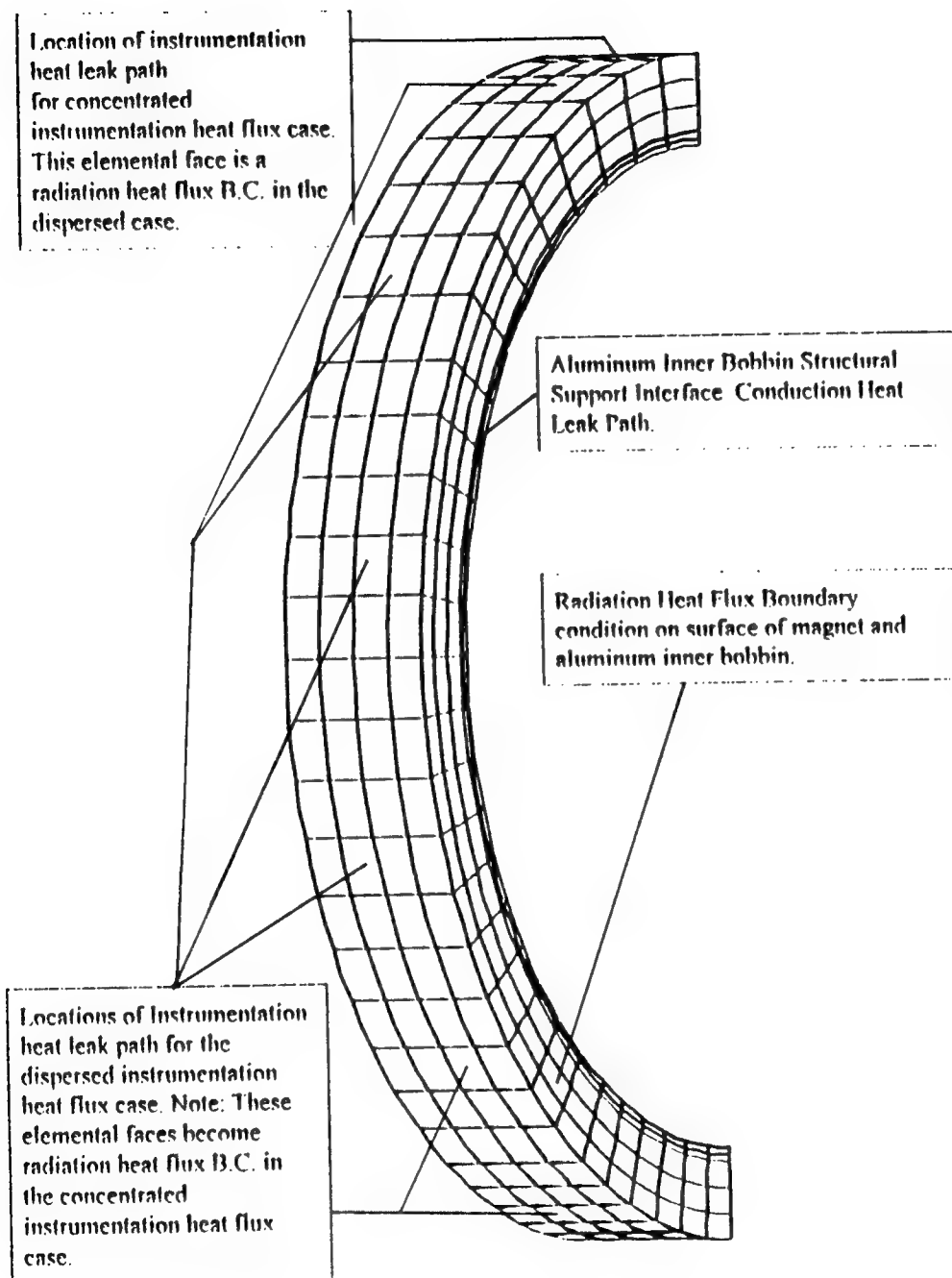


Figure 4: Wire Diagram of View 3 of Bisected SCM

Coefficients for Eqn. of Form: $K = a + bT + cT^2 + dT^3 + eT^4$					
Eqn.	a	b	c	d	e
Magnet Axial (k_z)	0.20629	4.8E-02	N/A	N/A	N/A
Magnet Radial (k_r)	0.16354	9.8E-03	N/A	N/A	N/A
Magnet Azimuth (k_θ)	-879.117	592.241	-2.95E01	4.39E-01	N/A
Al Inner Bobbin $k_r = k_z$ $= k_\theta$	-0.4586	13.0864	0.18898	-10E-03	7.9E-05

Table 2: Thermal Conductivities for SCM Components

The SCM model was created using the DISPLAY III portion of NISA [Ref. 19]. The magnet and the aluminum inner bobbin were first structured by linking together six 30-degree azimuthal sectors. NISA refers to these azimuthal sectors as hyperpatches. A custom mesh of 3-D solid parabolic elements, each containing 20 nodes, was arranged to maintain nodal continuity while still remaining within the bounds imposed by the cylindrical coordinate limitations of NISA. The number of

axial elemental divisions was kept at four throughout the SCM. The magnet and the aluminum inner bobbin had different numbers of radial elemental divisions; two in the aluminum inner bobbin and three in the magnet. The number of azimuthal elemental divisions was varied over the six hyperpatches. An attempt was made to have a higher density of elements, and thus nodes, in the hyperpatch containing the cryocooler interface. Therefore, six azimuthal elemental divisions were placed in the cryocooler hyperpatch, reducing to five divisions in the next three hyperpatches and finally four divisions in the last two hyperpatches. Figure 5 shows how the number of elemental divisions and nodal densities varied in the model.

C. BOUNDARY CONDITIONS

The boundary conditions used in the thermal analysis were developed from information provided by NSWC, Annapolis. This included a table of heat leak contributors and their values and a cryocooler no-load performance curve (cooling capacity in Watts vs. temp. in degrees Kelvin) for the cryocooler. The cryocooler no-load performance curve is included as Figure 6. The table of heat leak contributors included 1.5 Watts for heat leak into the SCM during the initial cooling process from higher temperatures. This was disregarded under the assumption that this study handled an already cooled SCM.

The radiation heat leak from a 35 K environment into the SCM was assumed uniform over all exposed surfaces of the magnet and aluminum inner bobbin. The only portions of the surface area of the control volume not exposed to radiation are the circular edge of the structural support end of the aluminum inner bobbin, the cryocooler interface and those areas on the outer circumference of the magnet selected to represent instrumentation heat leak paths. The conductive

heat leak through the structural support interface on one end of the aluminum inner bobbin was also assumed uniform. Since the SCM is enclosed in the cryostat in a vacuum, there is no convective heat transfer.

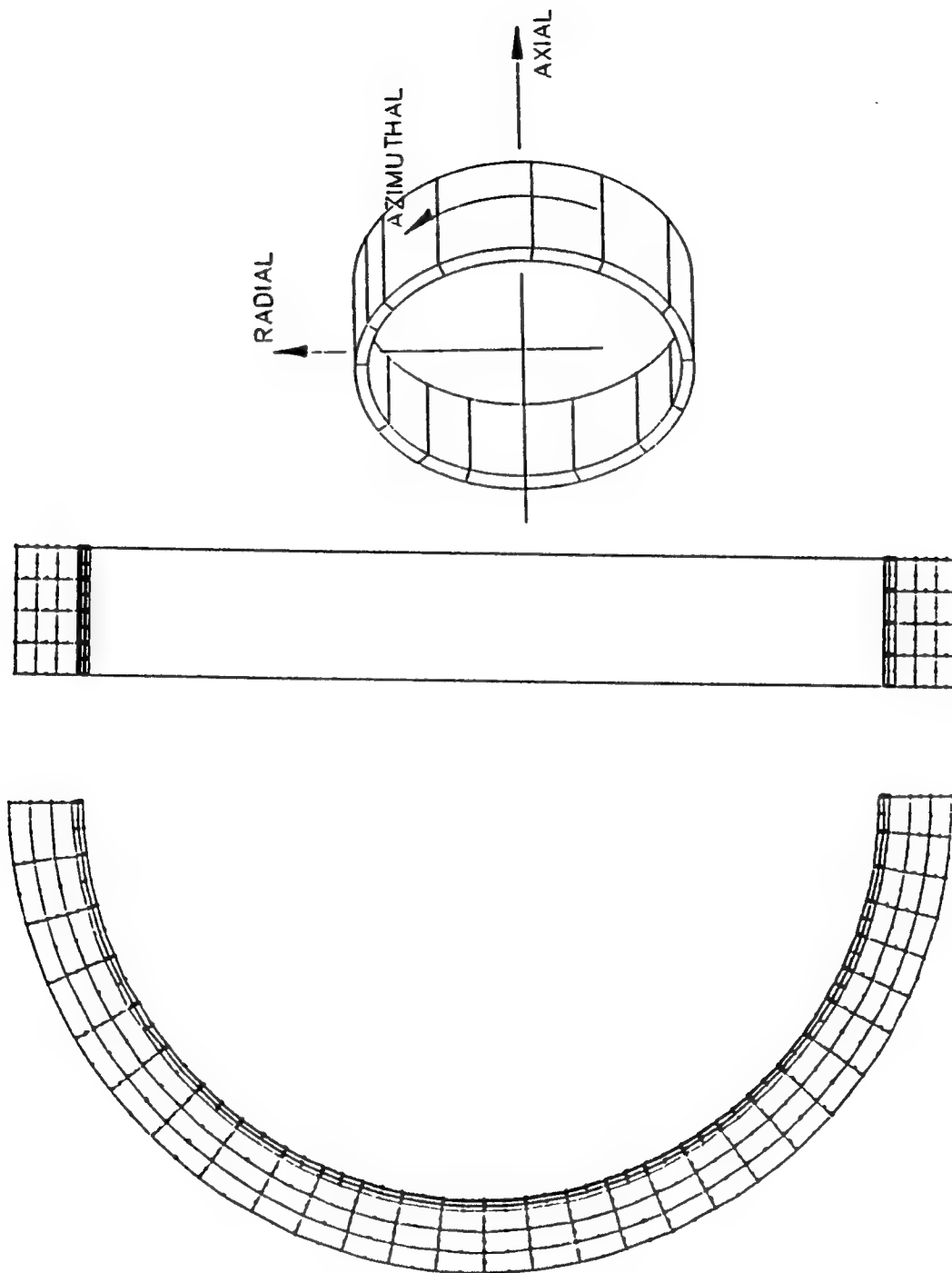


Figure 5: Arrangement of Elements and Nodes in Bisected SCM

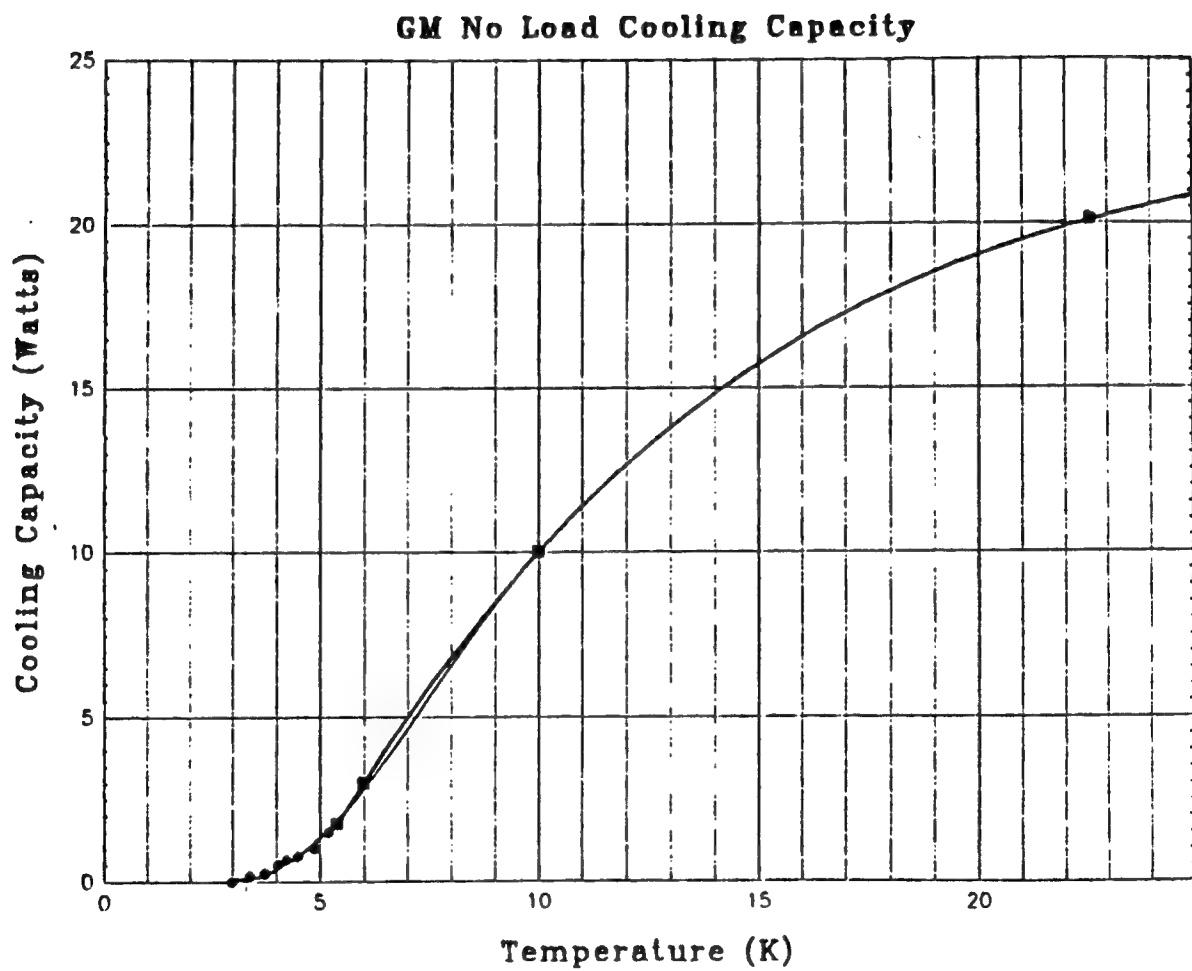


Figure 6: Cryocooler No-Load Performance Curve

Selection of the instrumentation heat leak path gave rise to the two major cases of this study:

i) In the dispersed instrumentation heat flux case, one outer facing element in each of the six azimuthal sectors was designated an instrumentation heat leak path. This equates to twelve total instrumentation heat leak paths in the actual non-bisected SCM.

ii) In the concentrated instrumentation heat flux case, one outer facing element in one of the azimuthal sectors was designated an instrumentation heat leak path. This was the sector diametrically opposite the sector containing the cryocooler interface. This equates to two total instrumentation heat leak paths in the actual non-bisected SCM. Additionally, it was adjacent to the plane of symmetry. In the actual non-bisected SCM, the two elemental faces combine to form a single area of instrumentation heat flux.

The previously discussed limitations on nodal density prevented a more realistic modeling of the instrumentation heat leak paths. The instrumentation heat flux elemental faces should have been on the scale of the cross section of typical instrumentation wiring (approximately 10-20 cm²). This would have resulted in a higher instrumentation heat flux for the same value of heat leak. In this regard, the concentrated instrumentation heat flux case (Inst. heat flux elemental face area of 116 cm²) is more realistic than the dispersed case (average inst. heat flux elemental face area of 196cm²).

Boundary conditions were modeled in NISA as elemental heat flux in W/m². They were obtained by dividing each heat leak value in Watts by the applicable surface area (in m²) of its heat leak path boundary on the non-bisected SCM. A negative elemental heat flux value in NISA equates to heat leak into the element. Zero W/m² values were entered on the elemental faces in the plane of symmetry. The boundary condition at the cryocooler interface was not a heat flux, but

a specified nodal temperature in degrees Kelvin, based on the cryocooler no-load performance curve.

Heat Leak	Value	Boundary	Area	Heat Flux
Radiation	0.25 W	Outer Surfaces	6.167 m ²	0.0405 W/m ²
Cond.	0.25 W	Al Support	0.157 m ²	1.592 W/m ²
Instru- mentation	0.16 W	Misc. Wiring	0.177 m ²	1.362 W/m ²
Cryocooler Interface Nodal Temp. = 4.25 degrees Kelvin				

Table 3: Dispersed Inst. Heat Flux Case B.C. Data

Heat Leak	Value	Boundary	Area	Heat Flux
Radiation	0.25 W	Outer Surfaces	6.262 m ²	0.0399 W/m ²
Cond.	0.25 W	Al Support	0.157 m ²	1.592 W/m ²
Instru- mentation	0.16 W	Misc. Wiring	0.0232 m ²	6.902 W/m ²
Cryocooler Interface Nodal Temp. = 4.25 degrees Kelvin				

Table 4: Concentrated Inst. Heat Flux Case B.C. Data

III. RESULTS

A. GENERAL

In both of the two major cases the temperature in the SCM stayed well below the quench temperature of 11 degrees Kelvin. The results of each of these major cases will be presented by three different graphical views of the SCM's temperature profile and appropriate interpretive discussion. The views were selected to provide a look at the key areas of the SCM. The intent of the commentary is to link the characteristics of the SCM and the case boundary conditions with what is seen in the profiles.

B. DISPERSED INSTRUMENTATION HEAT FLUX CASE

The maximum temperature reached in the SCM is 4.491 K, occurring at a node in the outer circumference of the magnet. Figure 7 shows view 1 with the cryocooler interface and the effect of its low temperature on adjacent elements in both the aluminum inner bobbin and the magnet. The isotherms in the aluminum inner bobbin are striped in the axial direction because of the isotropic nature of that material's thermal conductivity. Seen in both the upper and lower symmetry plane, are axial isotherms curved radially inward because of the instrumentation heat flux on the outer circumference of the magnet. Figure 8 shows view 2 and the structural support interface side of the aluminum inner bobbin. The effect of this conductive heat leak path does not appear very dramatic. Figure 9 shows view 3 of the SCM with bands of constant temperature running in an azimuthal direction on the outer circumference of the magnet. This illustrates the dominance of the azimuthal component of the magnet's thermal conductivity, which runs parallel to the Nb-Ti wires. This is also indicative of the effect of dispersed areas of

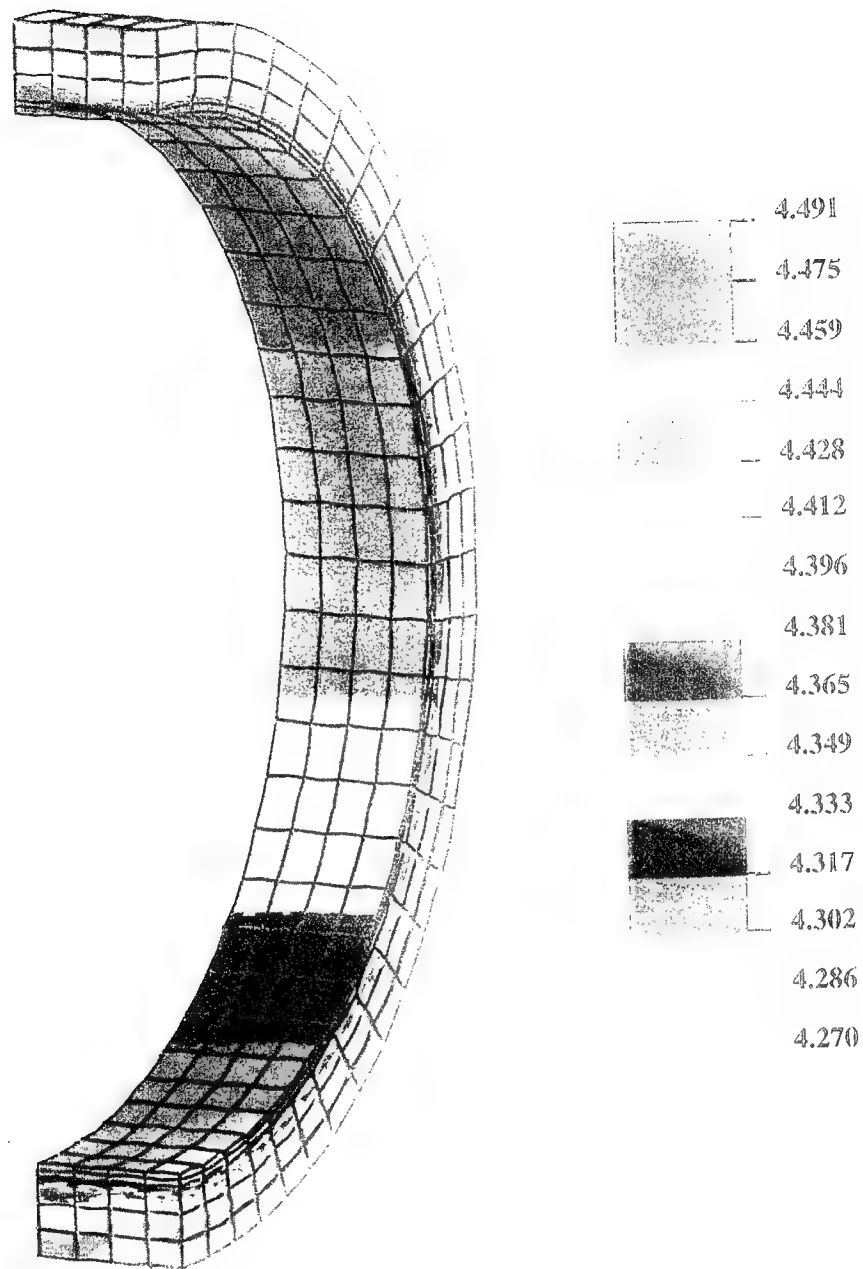


Figure 7: Dispersed Instrumentation Heat Flux Case
Temperature Profile (View 1)

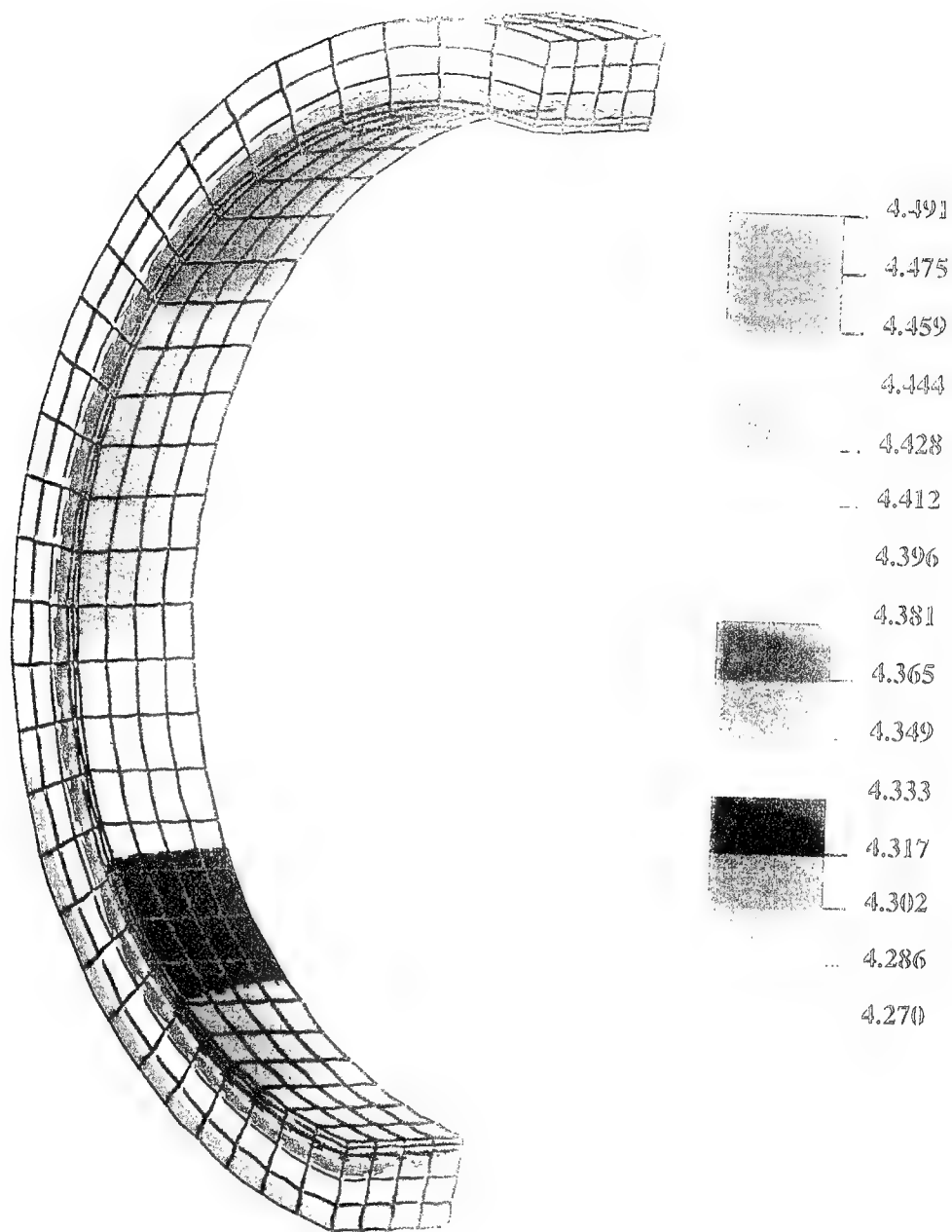


Figure 8: Dispersed Instrumentation Heat Flux Case
Temperature Profile (View 2)

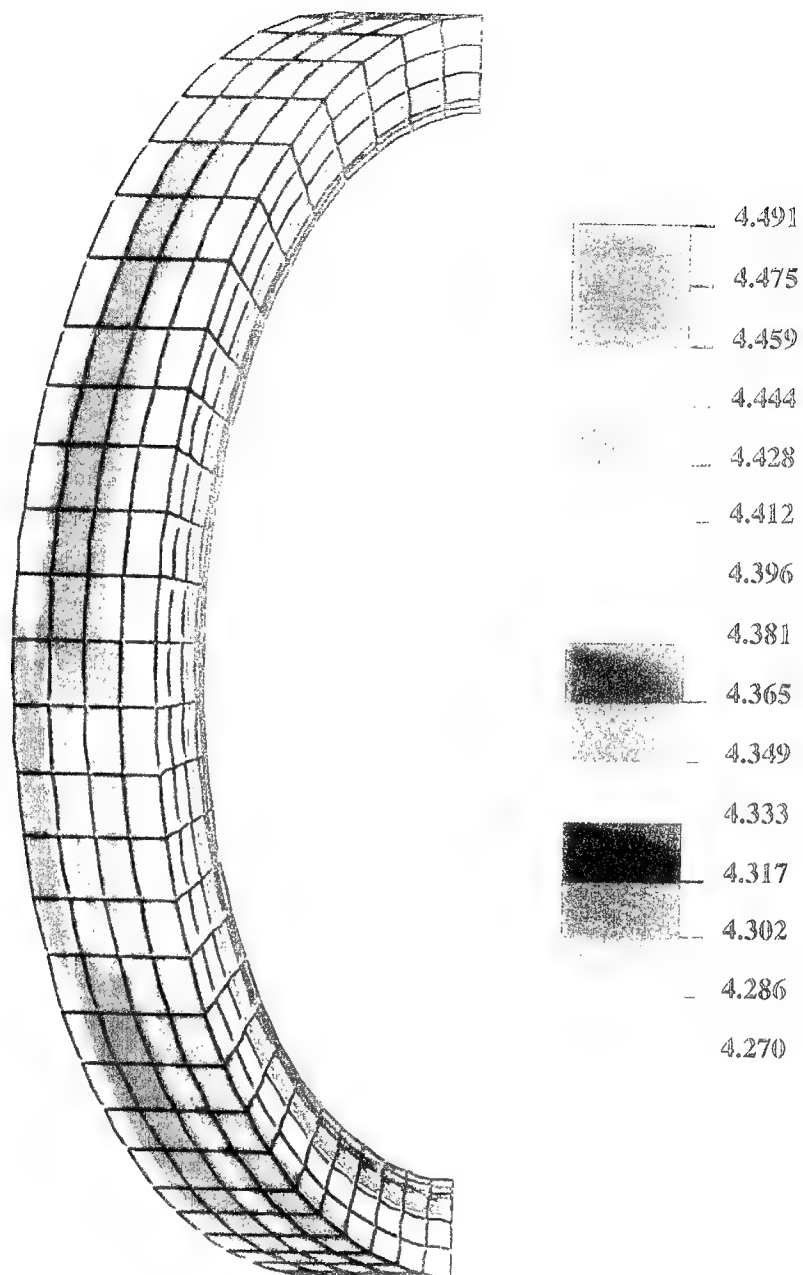


Figure 9: Dispersed Instrumentation Heat Flux Case
Temperature Profile (View 3)

instrumentation heat flux. The temperature gradient is much greater in the axial and radial directions which run perpendicular to the wires. The differences in the axial and radial temperature gradients, though slight, are attributable to the rectangular shape of the Nb-Ti wires. The long axis of the 1.0mm by 0.5mm Nb-Ti wire is aligned parallel to the axial direction of the magnet. This results in the axial thermal conductivity being about twice that of the radial thermal conductivity for any given temperature.

C. CONCENTRATED INSTRUMENTATION HEAT FLUX CASE

The maximum temperature in the SCM is 4.460 K occurring, again, in the outer circumference of the magnet. The same general observations can be made on this case's temperature profiles as were made on the dispersed case. Figure 10 shows view 1. The lower symmetry plane isotherms near the cryocooler interface are no longer curved radially inward. They are nearly straight across in the axial direction. This is because there is no longer any instrumentation heat flux elements in that hyperpatch. The upper symmetry plane, however, has an isothermal pattern with increased gradients and gives evidence of the presence of the concentrated instrumentation heat flux element. Figure 11 shows view 2 and an apparent decrease in the radial gradient as compared to the dispersed case. This makes sense based on the absence of the high heat flux boundary conditions along the outer circumference of the magnet. Figure 12 shows view 3 and the thermal pattern on the outer circumference of the magnet, which reveals the location of the instrumentation heat flux element. The high temperature isotherms are grouped in the upper azimuthal sector of the bisected SCM. The majority of the outer circumferential elemental faces are at a constant temperature.

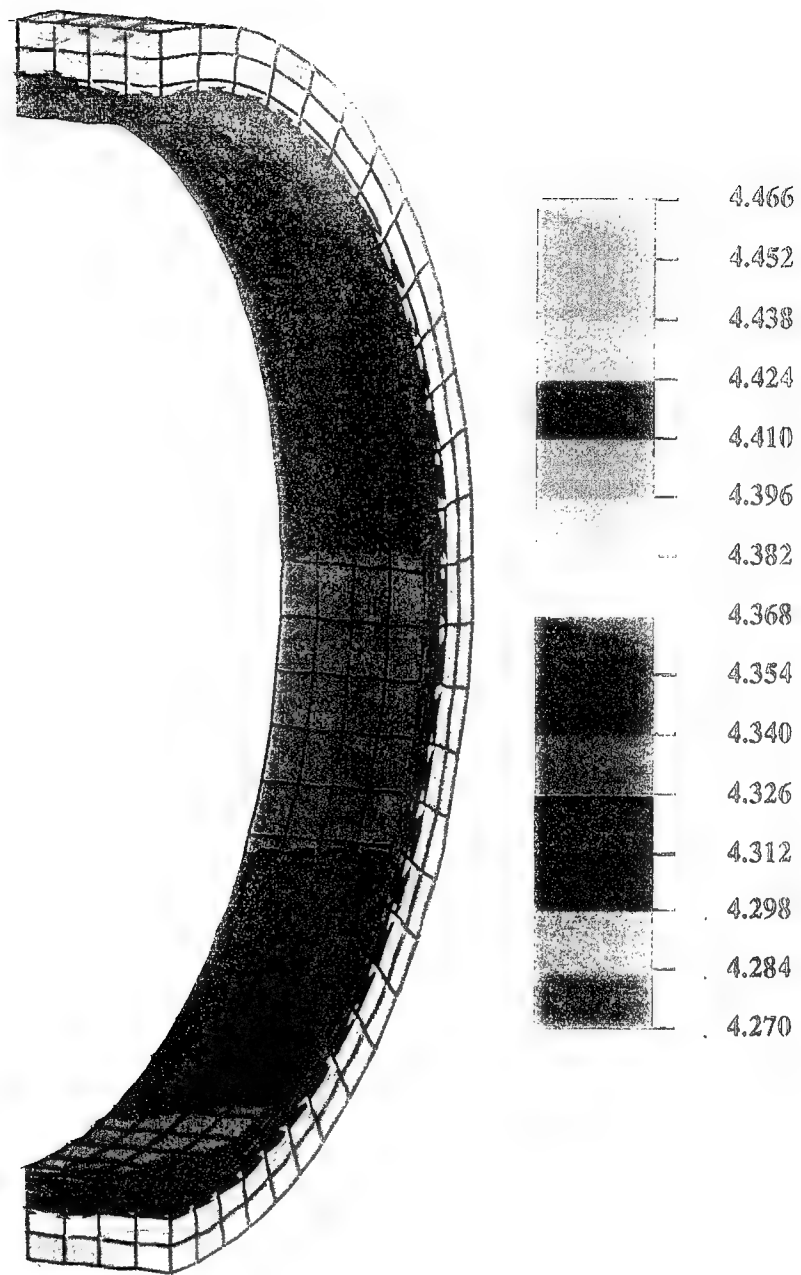


Figure 10: Concentrated Instrumentation Heat Flux Case
Temperature Profile (View 1)

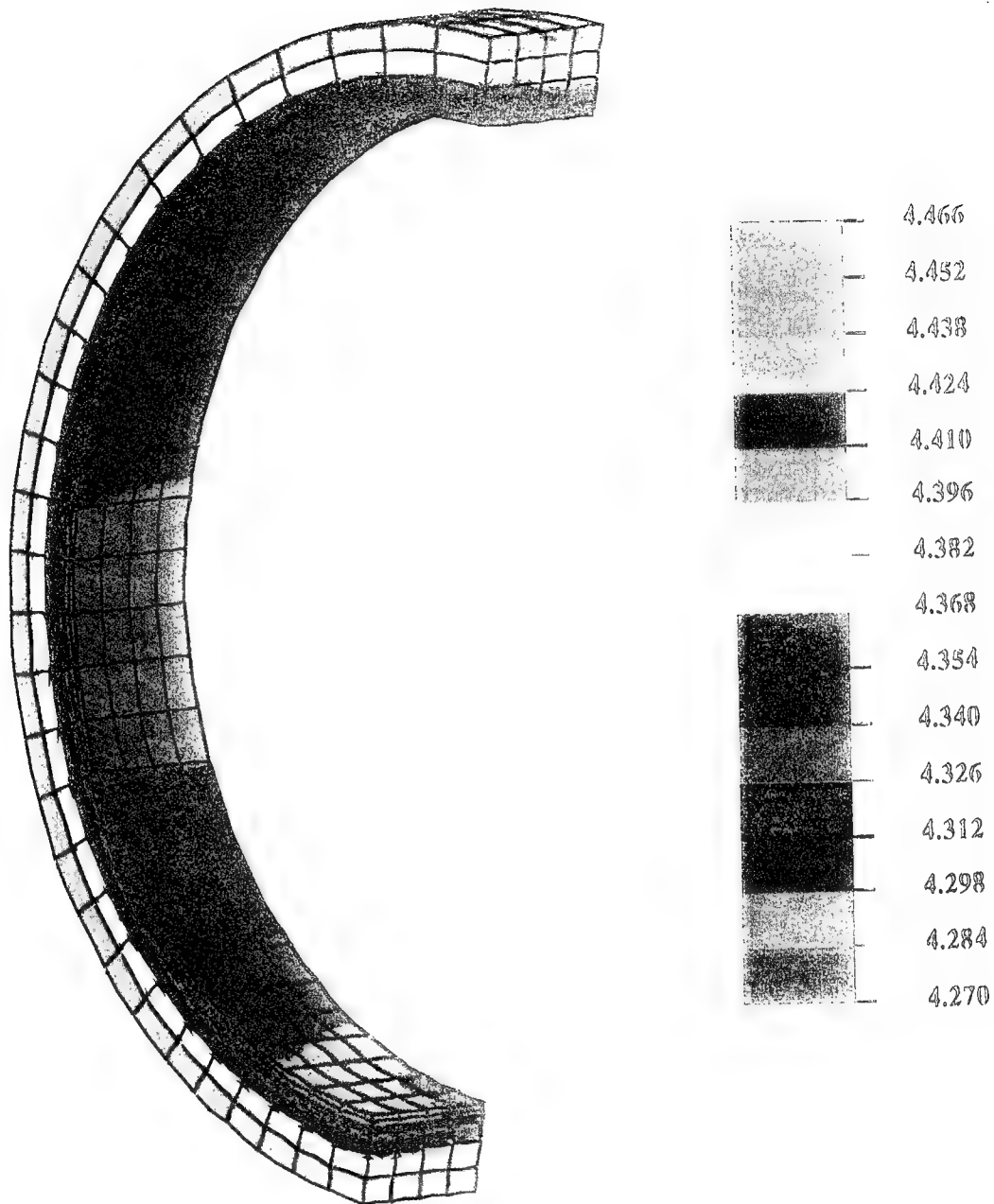


Figure 11: Concentrated Instrumentation Heat Flux Case
Temperature Profile (View 2)

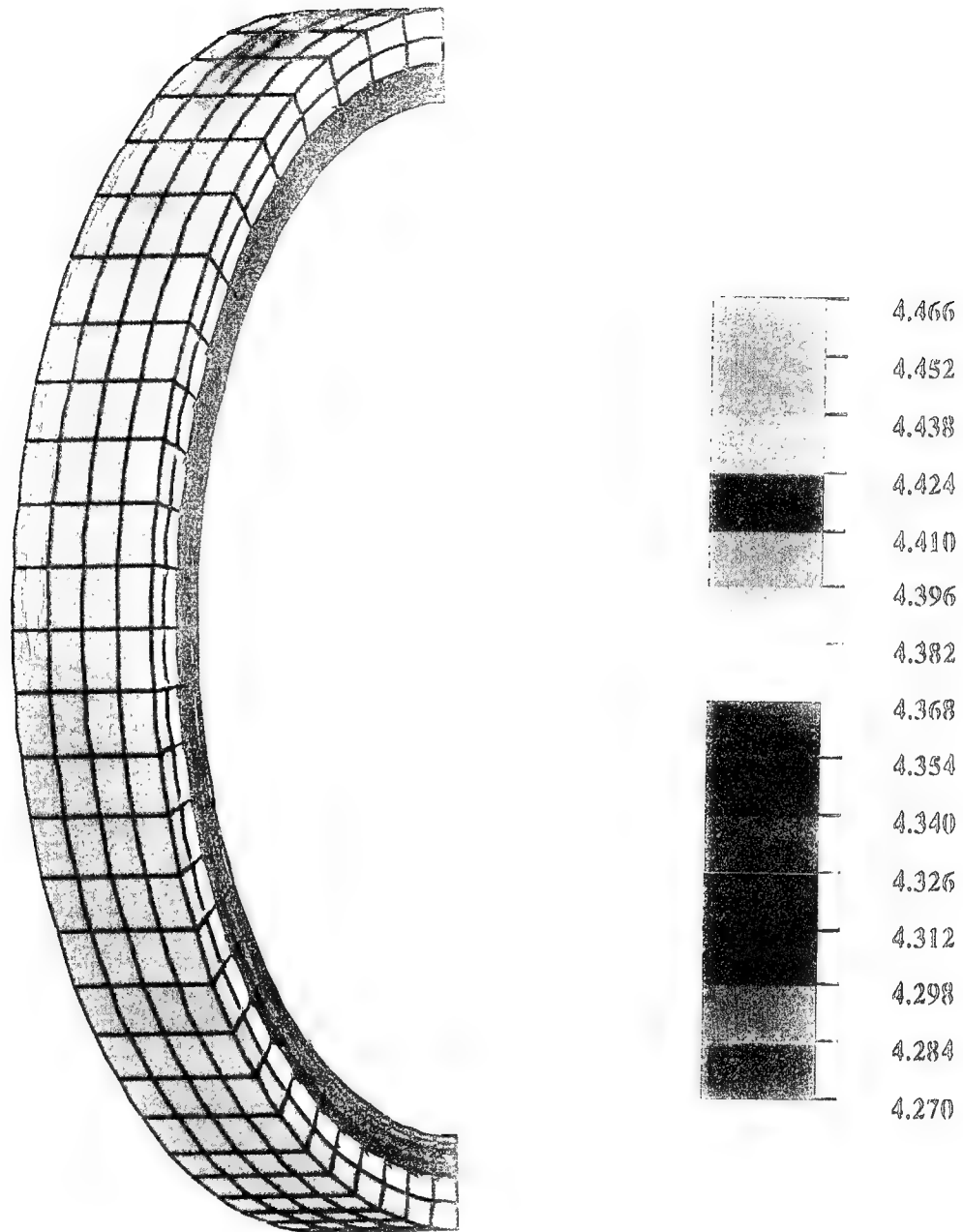


Figure 12: Concentrated Instrumentation Heat Flux Case
Temperature Profile (View 3)

D. EXPLORATORY QUENCH CASES

The heat leak values used in the two major cases are only preliminary design estimates given to NSWC by the ALISS design contractor. It was considered beneficial to explore what levels of these heat leaks would quench the SCM. The values of instrumentation heat leak, radiation heat leak and conductive heat leak were each separately raised until an SCM nodal temperature reached approximately 11 K. In each of the exploratory cases, two of the heat leak values were held constant at the preliminary design estimate value while the third heat leak value was raised. The instrumentation heat flux locations of the concentrated instrumentation heat flux case were used. Table 5 shows the results of these exploratory cases. Noteworthy is that, as total heat leak increased, the cryocooler interface temperature increased as obtained from the no-load performance curve. The ΔT between the cryocooler interface temperature and the highest temperature in the SCM remained fairly constant at less than 1 degree K.

Heat Leak Variable	Cryocooler Interface Temp.	Heat Leak Value at Quench
Instrumentation Heat Leak	10.6 K	10.4 W
Radiation Heat Leak	10.5 K	10.3 W
Conduction Heat Leak	10.7 K	10.6 W

Table 5: Exploratory Case Results

IV. DISCUSSION

The results of this thesis have established a foundation and background for future NPS heat transfer study of the ALISS SCM.

A. CONCLUSIONS

- the cryocooler is able to maintain the SCM below the quench temp.
- the highest temp always occurred near the instrumentation heat leak boundaries.
- the current version of NISA is not well suited for thermally analyzing orthotropic materials in a cylindrical coordinate system.

B. RECOMMENDATIONS

- further research should examine transient conditions during the initial cooling down of the SCM or during minesweep operations.
- use software able to accept orthotropic thermal conductivities in a cylindrical coordinate system, so that a finer mesh can be used.
- if a finer mesh can be used, remodel the instrumentation heat flux elemental faces to reflect the cross-sectional area of typical instrumentation wiring.

LIST OF REFERENCES

1. Melia, Tamara Moser, "Damn the Torpedoes: A Short History of U.S. Naval Mine Countermeasures, 1777-1991," p. 129, Naval Historical Center, Washington, D. C., 1991.
2. Melia, Tamara Moser, "Damn the Torpedoes: A Short History of U.S. Naval Mine Countermeasures, 1777-1991," p. 134, Naval Historical Center, Washington, D. C., 1991.
3. Mundy, Carl E., Gen., USMC, "Thunder and Lightning: Joint Littoral Warfare," p. 45, Joint Forces Quarterly, Spring 1994.
4. Mundy, Carl E., Gen., USMC, "Strategy for a New Era," p. 57, The Retired Officer Magazine, November 1994.
5. Brown, David K., Royal Corps of Naval Constructors, "Damn the Mines!," p. 45, U.S. Naval Institute Proceedings, March, 1992.
6. Melia, Tamara Moser, "Damn the Torpedoes: A Short History of U.S. Naval Mine Countermeasures, 1777-1991," p. 136, Naval Historical Center, Washington, D. C., 1991.
7. Dr. J. Walters, et. al., "Applications of Superconductivity to Shallow Water Minesweeping," Naval Engineers Journal, Vol. 104, No. 3, p. 53, May 1992.
8. Superconductivity and its Applications, Williams, J.E.C, Pion Limited, London, 1970.
9. A Guide to Superconductivity, Fishlock, D., American Elsevier Publishing Co., Inc., 1969.
10. Earlier and Recent Aspects of Superconductivity, Bednorz, J.G., Muller, K. A., Springer-Verlag, 1990.
11. Lusk, M. A., et. al., "The Fabrication of a Ceramic Superconducting Wire, "Superconductor Science and Technology, Vol. 1, No. 3, 1988.
12. "Proceedings of the Workshop on Naval Applications of Superconductivity, Nov. 4-6, 1970, Naval Ship Research and Development Laboratory, Panama City, FL." July 1, 1971, Naval Research Laboratory, Washington, D. C.
13. Dr. J. Walters, et. al., "Applications of Superconductivity to Shallow Water Minesweeping," Naval Engineers Journal, Vol. 104, No. 3, p. 59, May 1992

14. NISA Users Manual, NISA Version 93.0, Engineering Mechanics Research Corporation, Troy, MICH, 1993.
15. Private Communication with Dr. J. Walters of Annapolis Detachment, CDNSWC.
16. Touloukian, Y. S., Thermophysical Properties of Matter, Thermophysical Properties Research Center, Purdue University, IFI/Plenum Data Corp., N. Y., 1970.
17. Table Curve Software, AISN Software, 1990.
18. Private Communication with Dr. J. Walters of Annapolis Detachment, CDNSWC.
19. Egan, J. P., Boom, R. W. "Measurements of Electrical Resistivity and Thermal Conductivity of High Purity Aluminum in Magnetic Fields",
20. Display III Users Manual, NISA Version 93.0, Engineering Mechanics Research Corporation, Troy, MICH, 1993.

INITIAL DISTRIBUTION LIST

	No. Copies
1. Defense Technical Information Center Cameron Station Alexandria, Virginia 22304-6145	2
2. Library, Code 52 Naval Postgraduate School Monterey, California 93943-5101	2
3. Department Chairman, Code ME/Kk Department of Mechanical Engineering Naval Postgraduate School Monterey, California 93943-5002	2
4. Naval/Mechanical Engineering Curricular Office Naval Postgraduate School Code 34 Monterey, California 93943-5002	1
5. Professor Matthew D. Kelleher Department of Mechanical Engineering Naval Postgraduate School Monterey, California 93940	2
6. Magnetic ALISS Office (Code 813) Annapolis Detachment, Carderock Division Naval Surface Warfare Center Annapolis, Maryland 21402-5067	2
7. LT Phillip K. Pall 201 Glenwood Circle Apt.11A Monterey, California 93940	2